NATIONAL ADVISORY COMMITTEE FOR AERONAUTICS

REPORT No. 763

TESTS OF AIRFOILS DESIGNED TO DELAY THE COMPRESSIBILITY BURBLE

By JOHN STACK

1943

For sale by the Superintendent of Documents, U. S. Government Printing Office, Washington 25, D. C. . . . . Price 15 cents.

AERONAUTIC SYMBOLS

1. FUNDAMENTAL AND DERIVED UNITS

	Symbol	Metric		English	
		Unit	Abbreviation	Unit	Abbreviation
Length	l	meter	m	foot (or mile)	ft (or mi)
Time	t	second	s	second (or hour)	sec (or hr)
Force	F	weight of 1 kilogram	kg	weight of 1 pound	lb
Power	P	horsepower (metric)		horsepower	hp
Speed	V	kilometers per hour	kph	miles per hour	mph
		meters per second	mps	feet per second	fps

2. GENERAL SYMBOLS

W Weight$=mg$

g Standard acceleration of gravity$=9.80665$ m/s^2 or 32.1740 ft/sec^2

m Mass$=\frac{W}{g}$

I Moment of inertia$=mk^2$. (Indicate axis of radius of gyration k by proper subscript.)

μ Coefficient of viscosity

ν Kinematic viscosity

ρ Density (mass per unit volume)

Standard density of dry air, 0.12497 kg-m^{-4}-s^2 at 15° C and 760 mm; or 0.002378 lb-ft^{-4} sec^2

Specific weight of "standard" air, 1.2255 kg/m^3 or 0.07651 lb/cu ft

3. AERODYNAMIC SYMBOLS

S Area

S_w Area of wing

G Gap

b Span

c Chord

A Aspect ratio, $\frac{b^2}{S}$

V True air speed

q Dynamic pressure, $\frac{1}{2}\rho V^2$

L Lift, absolute coefficient $C_L=\frac{L}{qS}$

D Drag, absolute coefficient $C_D=\frac{D}{qS}$

D_0 Profile drag, absolute coefficient $C_{D0}=\frac{D_0}{qS}$

D_i Induced drag, absolute coefficient $C_{Di}=\frac{D_i}{qS}$

D_p Parasite drag, absolute coefficient $C_{Dp}=\frac{D_p}{qS}$

C Cross-wind force, absolute coefficient $C_C=\frac{C}{qS}$

i_w Angle of setting of wings (relative to thrust line)

i_t Angle of stabilizer setting (relative to thrust line)

Q Resultant moment

Ω Resultant angular velocity

R Reynolds number, $\rho\frac{Vl}{\mu}$ where l is a linear dimension (e.g., for an airfoil of 1.0 ft chord, 100 mph, standard pressure at 15° C, the corresponding Reynolds number is 935,400; or for an airfoil of 1.0 m chord, 100 mps, the corresponding Reynolds number is 6,865,000)

α Angle of attack

ϵ Angle of downwash

α_0 Angle of attack, infinite aspect ratio

α_i Angle of attack, induced

α_a Angle of attack, absolute (measured from zero-lift position)

γ Flight-path angle

REPORT No. 763

TESTS OF AIRFOILS DESIGNED TO DELAY THE COMPRESSIBILITY BURBLE

By JOHN STACK

Langley Memorial Aeronautical Laboratory

Langley Field, Va.

National Advisory Committee for Aeronautics

Headquarters, 1500 New Hampshire Avenue NW., Washington 25, D. C.

Created by act of Congress approved March 3, 1915, for the supervision and direction of the scientific study of the problems of flight (U. S. Code, title 49, sec. 241). Its membership was increased to 15 by act approved March 2, 1929. The members are appointed by the President, and serve as such without compensation.

REPORT No. 763

TESTS OF AIRFOILS DESIGNED TO DELAY THE COMPRESSIBILITY BURBLE

By JOHN STACK

SUMMARY

Fundamental investigations of compressibility phenomena for airfoils have shown that serious adverse changes of aerodynamic characteristics occur as the local speed over the surface exceeds the local speed of sound. These adverse changes have been delayed to higher free-stream speeds by development of suitable airfoil shapes. The method of deriving such airfoil shapes is described, and aerodynamic data for a wide range of Mach numbers obtained from tests of these airfoils in the Langley 24-inch high-speed tunnel are presented. These airfoils, designated the NACA 16-series, have increased critical Mach number. The same methods by which these airfoils have been developed are applicable to other airplane components.

INTRODUCTION

Development of airfoil sections suitable for high-speed applications has generally been difficult because little was known of the flow phenomenon that occurs at high speeds. A definite critical speed has been found at which serious detrimental flow changes occur that lead to serious losses in lift and large increases in drag. This flow phenomenon, called the compressibility burble, was originally a propeller problem but, with the development of high-speed aircraft, serious consideration has to be given to other parts of the airplane. It is important to realize, however, that the propeller will continue to offer the most serious compressibility problems for two reasons: First, because propeller-section speeds are higher than the speed of the airplane and, second, because structural requirements lead to thick sections near the root.

Fundamental investigations of high-speed air-flow phenomena recently completed (references 1 to 3) have provided much new information. From practical considerations an important conclusion of these investigations has been the determination of the critical speed, that is, the speed at which the compressibility burble occurs. The critical speed was shown to be the translational velocity at which the sum of the translational velocity and the maximum local induced velocity at the surface of the airfoil or other body equals the local speed of sound. Obviously, then, higher critical speeds can be attained through the development of airfoils that have minimum induced velocity for any given value of the lift coefficient.

Presumably, the highest critical speed will be attained by an airfoil that has uniform chordwise distribution of induced velocity or, in other words, a flat pressure-distribution curve. All conventional airfoils tend to have high negative pressures and correspondingly high induced velocities near the nose, which gradually taper off to the air-stream conditions at the rear of the airfoil. If the same lift coefficient can be obtained by decreasing the induced velocity near the nose and increasing the induced velocity over the rear portion of the airfoil, the critical speed will be increased by an amount proportional to the decrease obtained in the maximum induced velocity. The ideal airfoil for any given high-speed application is, then, that shape which at its operating lift coefficient has uniform chordwise distribution of induced velocity. Accordingly, an analytical search for such airfoils has been conducted by members of the staff of the Langley Memorial Aeronautical Laboratory and these airfoils have been investigated experimentally in the Langley 24-inch high-speed tunnel.

The first airfoils investigated showed marked improvement over those shapes already available; not only was the critical speed increased but also the drag at low speeds was decreased considerably. Because of the marked improvement achieved, it was considered desirable to extend the thickness and the lift-coefficient ranges for which the original airfoils had been designed to obtain data of immediate practical value before further extending the investigation of the fundamental aspects of the problem.

SYMBOLS

x	abscissa of camber line
y_c	ordinate of camber line
t	thickness, percent of chord
c	airfoil chord
θ	defined by $\frac{x}{c}=\frac{1}{2}(1-\cos\theta)$
C_L	lift coefficient
C_D	drag coefficient
$C_{D_{min}}$	minimum drag coefficient
$C_{m_{c/4}}$	pitching-moment coefficient about quarter-chord point
P	pressure coefficient
M	Mach number
M_{cr}	critical Mach number
R	Reynolds number
α	angle of attack, degrees

736080—47

DEVELOPMENT OF AIRFOIL SERIES

The aerodynamic characteristics of any airfoil are, in general, dependent upon the airfoil camber line and the thickness form. Mean camber lines were derived analytically to obtain a uniform chordwise distribution of induced velocity or pressure for certain designated lift coefficients, and an analytical search for a thickness form that likewise has low and uniform chordwise induced-velocity distribution was then undertaken.

Derivation of the camber line.—Glauert (reference 4) has derived expressions for the local induced velocity at a point on an airfoil (zero thickness assumed) in terms of the circulation around an airfoil corresponding to a certain distribution of vorticity along the airfoil surface. By assuming the distribution of vorticity to be constant, a line airfoil is determined that gives uniform chordwise pressure distribution. The form of the equation so derived is

$$\frac{y_c}{C_L}=\frac{1}{4\pi}\left(\log\frac{1}{1-x}+x\log\frac{1-x}{x}\right) \tag{1}$$

where y_c is the ordinate of the mean camber line, x is the abscissa, and the chord is taken as unity. The idealized form described by this equation has discontinuities at the nose and at the tail. This difficulty is circumvented by assuming very slight gradients in the chordwise load distribution just at the nose and just at the tail. This form, derived by using the Fourier series method, is given by the equation

$$\frac{y_c}{c}=\frac{C_L}{4\pi}(0.3833-0.3333\cos 2\theta-0.0333\cos 4\theta$$
$$-0.0095\cos 6\theta-0.0040\cos 8\theta$$
$$-0.0020\cos 10\theta-0.0012\cos 12\theta) \tag{2}$$

where $\frac{x}{c}=\frac{1}{2}(1-\cos\theta)$ and c is the airfoil chord.

Equation (2) expresses the mean camber line chosen for airfoils of the series developed. Load or induced-velocity gradings derived from both equations (1) and (2) are actually identical for all practical purposes. Mean-camber-line ordinates are given in table I for $C_L=1.0$.

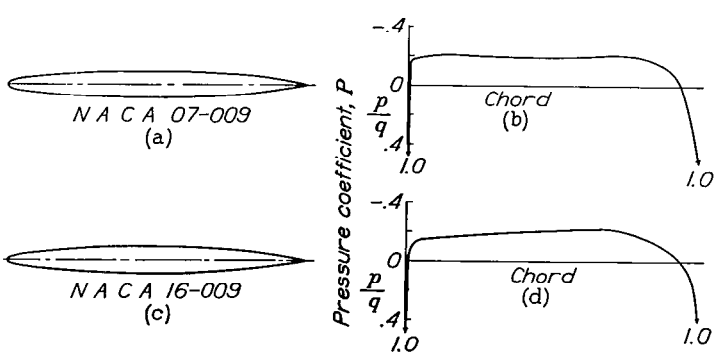

FIGURE 1.—Basic airfoils and theoretical pressure distributions.

In order to obtain the mean camber line giving uniform chordwise distribution of induced velocity for other values of the lift coefficient, the values given in table I are multiplied by the value of the desired lift coefficient.

TABLE I

CAMBER-LINE ORDINATES FOR NACA 16- AND 07-SERIES AIRFOILS WITH $C_L=1.0$

[All values measured in percent chord from chord linel

Station	Ordinate	Slope
0	0	0.62234
1.25	.535	.34771
2.5	.930	.29155
5	1.580	.23432
7.5	2.120	.19993
10	2.587	.17486
15	3.364	.13804
20	3.982	.11032
25	4.475	.08743
30	4.861	.06743
40	5.356	.03227
50	5.516	0
60	5.356	.03227
70	4.861	.06743
80	3.982	.11032
90	2.587	.17486
95	1.580	.23432
100	0	.62234

Derivation of the thickness form.—The derivation of the thickness form is not so simple or direct as the derivation of the mean camber line. The theoretical pressure distribution was computed by the methods of reference 5 for each of the several thickness forms investigated in reference 6. Some of these forms approached the desired shape but further modifications were investigated analytically and, finally, two shapes were chosen for tests. These shapes, the NACA 07–009 and the NACA 16–009, and the theoretical pressure distribution for each are shown in figure 1. The complete airfoil profile is derived by first calculating the mean camber line for the desired lift coefficient and then laying out the thickness ordinates given in table II from the camber line along perpendiculars to this line.

Airfoil designation.—Because the ideal series of airfoils requires an extremely large variation of shape, it becomes practically impossible to use previous numbering systems and, further, because this new series of airfoils is designed to obtain a specific pressure diagram, these airfoils are designated by a new series of numbers that is related to the flow and the operating characteristics of the airfoil. The first number is a serial number that describes the class of pressure distribution, the second number gives the location of the maximum negative pressure in percent of chord from the leading edge, the first number following the dash gives the lift coefficient for which the airfoil was designed to operate, and the last two numbers give the airfoil thickness in percent of chord. Thus the NACA 16–509 airfoil has the shape of the NACA 16–009 disposed about the uniform chordwise load camber line designed for a lift coefficient of 0.5.

TABLE II

THICKNESS ORDINATES FOR AIRFOILS WITH THICKNESS 9 PERCENT OF CHORD [1]

[All values measured in percent chord from and perpendicular to camber line]

Station	Ordinates	
	NACA 16-series airfoils	NACA 07-009 airfoil
0	0	0
1.25	.969	1.23
2.5	1.354	1.67
5	1.882	2.19
7.5	2.274	2.58
10	2.593	2.90
15	3.101	3.41
20	3.498	3.79
25	----------	4.07
30	4.063	4.27
40	4.391	4.46
50	4.500	4.50
60	4.376	4.37
70	3.952	4.00
80	3.149	3.34
90	1.888	1.91
95	1.061	1.00
100	.090	.09
Slope of radius through end of chord = $0.62234 C_L$		
L. E. radius of NACA 16-series airfoils = $0.396(t/0.09)^2$		

[1] For other thicknesses (t, in percent) multiply ordinates for NACA 16-series airfoils by $t/0.09$.

Airfoils investigated.—As previously stated, two basic airfoils were investigated. (See fig. 1.) The NACA 07–009 airfoil should, theoretically, give higher critical speed than the NACA 16–009 but an earlier investigation (reference 3) indicated that, for pressures occurring near the leading edge, the increase in the pressure coefficient as a result of compressibility effects was greater than that for pressures occurring farther back on the airfoil. Consequently, it was believed that, at speeds as high as the critical speed, the NACA 07–009 airfoil might have, as a result of compressibility effects, a pressure peak near the leading edge. The NACA 16–009 airfoil was therefore developed in an attempt to achieve the uniform chordwise load distribution at high speeds. Both forms were tested and the results showed higher drag and lower critical speed for the NACA 07–009 airfoil. Accordingly, the NACA 16–009 airfoil was chosen as the basic form for a series of airfoils designed to operate at various lift coefficients. For one value of the lift coefficient the effect of thickness variation was also investigated. The airfoils tested, of which profiles are shown in figure 2, are as follows:

NACA 16–009	NACA 16–506
NACA 16–109	NACA 16–512
NACA 16–209	NACA 16–515
NACA 16–509	NACA 16–521
NACA 16–709	NACA 16–530
NACA 16–1009	NACA 16–106
NACA 07–009	NACA 07–509

APPARATUS AND METHOD

The tests were conducted in the Langley 24-inch high speed tunnel, in which velocities approaching the speed of sound can be obtained. A brief description of this tunnel is given in reference 3. The balance measures lift, drag, and pitching moment and, except for improvements that permit a more accurate determination of the forces, is similar in principle to the balance used in the Langley 11-inch high-speed tunnel. The methods of operation are likewise similar to those employed in the operation of the Langley 11-inch high-speed tunnel (reference 7).

The models were of 5-inch chord and 30-inch span and were made of duralumin. A complete description of the method of constructing the models is given in reference 8. The model mounting is similar to that used in the Langley 11-inch high-speed tunnel (reference 7). The model extends across the tunnel and through holes cut in flexible brass end plates that preserve the contour of the tunnel walls. The holes are of the same shape as the model but are slightly larger than it is. The model ends are secured in the balance, which extends halfway around the test section and is enclosed in the airtight tunnel chamber similar to the installation in the Langley 11-inch high-speed tunnel (reference 7).

The speed range over which measurements were made extended, in general, from 25 percent of the speed of sound to values in excess of the critical speed. The corresponding

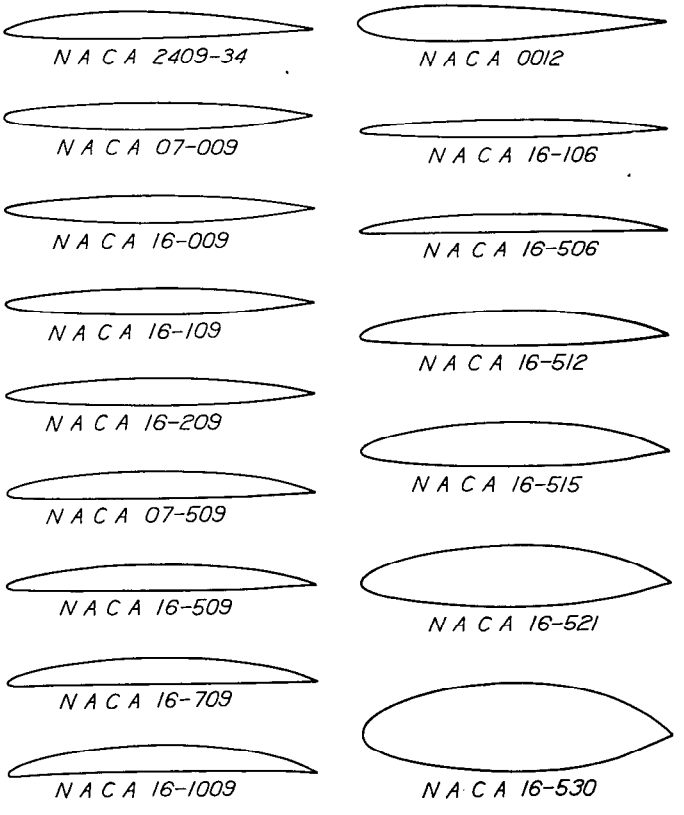

FIGURE 2.—Profiles for airfoils having high critical speeds.

Reynolds number range was from approximately 700,000 to nearly 2,000,000. The lift-coefficient range for which tests were made extended from zero lift for each airfoil to values approaching maximum lift.

PRECISION

Accidental errors are indicated by the scatter on the plots showing the measured test data (figs. 3 and 23 to 25). These errors are, in general, rather small and affect neither the application nor the comparison of the data. Tunnel effects arising from end leakage, restriction, and the usual type of tunnel-wall effect are important. Exact knowledge of these various effects is incomplete at the present time. The largest effects appear to arise from air leakage through the clearance between the model and the brass end plates in the tunnel wall through which the model passes. Investigations of the leakage effects have been made for the NACA 0012 airfoil with a special type of internal gap or clearance that permits wide variation of the gap. Data obtained with various gap settings of 0.01 inch and larger extrapolated to zero gap were used to evaluate the leakage correction for the standard type of mounting. These corrected data were then checked by means of wake-survey drag measurements with end leakage eliminated by rubber seals. Because the balance chamber is airtight, the end-leakage condition is related to the pressure distribution around the model. It was therefore considered advisable to check the method of correction for end leakage by wake-survey tests with end leakage eliminated by rubber seals for these new airfoils, which have radically different pressure distributions from the older airfoils such as the NACA 0012. Some of these data are shown in figure 3. In general, the agreement is excellent. The data have accordingly been corrected for end-leakage effects.

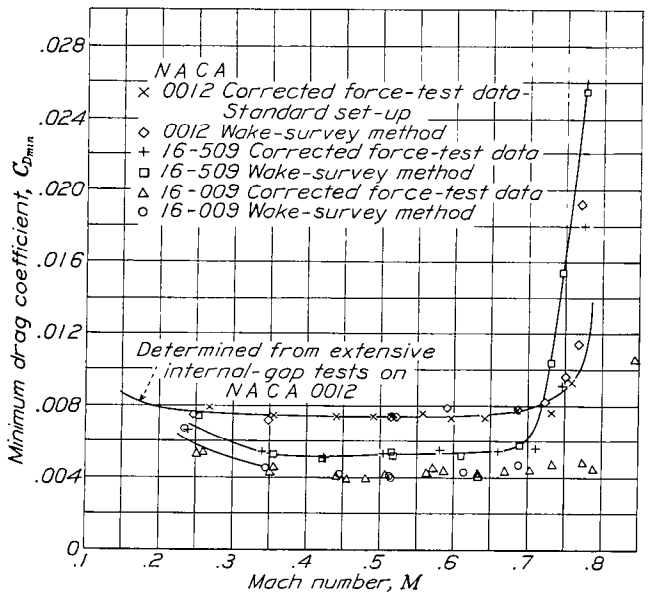

FIGURE 3.—Comparison of minimum drag obtained by various methods.

Other tunnel effects have not been completely investigated and the data have not been corrected for such effects as restriction or the more usual type of wall effect. As presented, the data are therefore conservative, inasmuch as investigations made thus far indicate that the coefficients are high and the critical speeds may be low. Strictly comparable data for two older airfoils, the 3C8 and the NACA 2409–34, for two Mach numbers are included so that comparisons can be made.

DISCUSSION

Aerodynamic characteristics for several of the NACA 16-series airfoils are given in figures 4 to 18. Examination of these figures indicates two important discrepancies between the theoretical design conditions and the data obtained from the tests: First, none of the airfoils attains the design lift coefficient at the design angle of attack (0°) and, second, the departure increases markedly with the design lift coefficient.

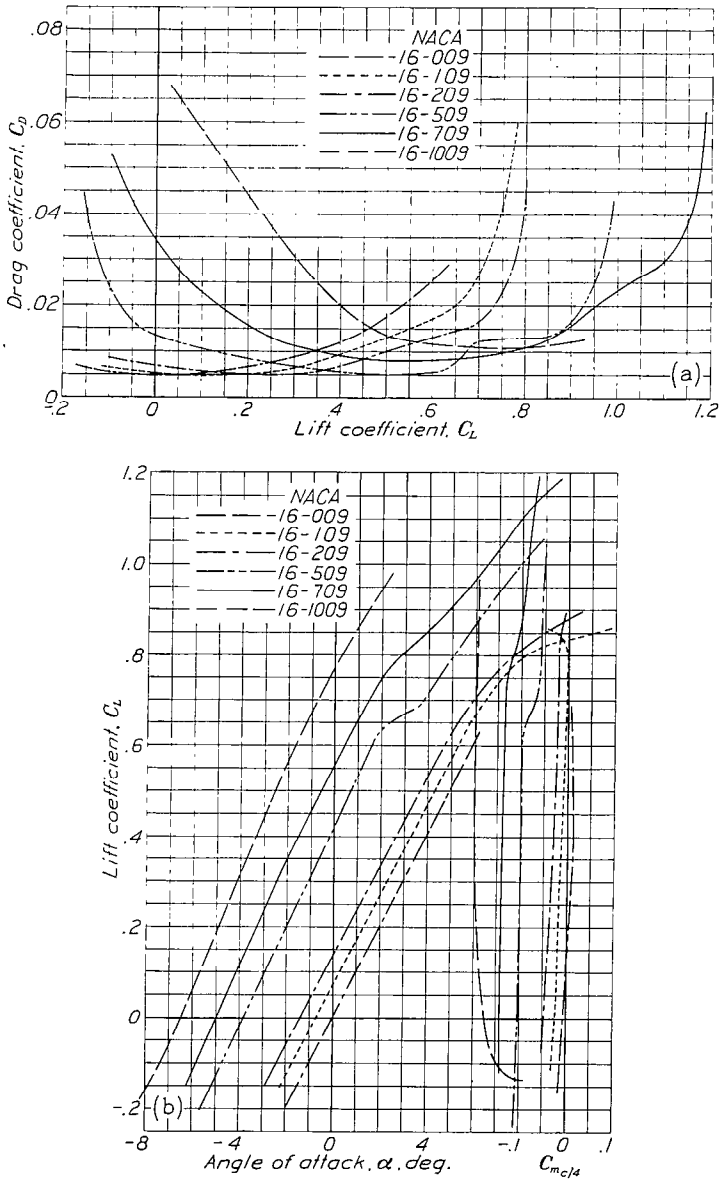

(a) Polar plots.
(b) Lift and moment data.

FIGURE 4.—Aerodynamic characteristics of NACA 16-009-series airfoils. M=0.30.

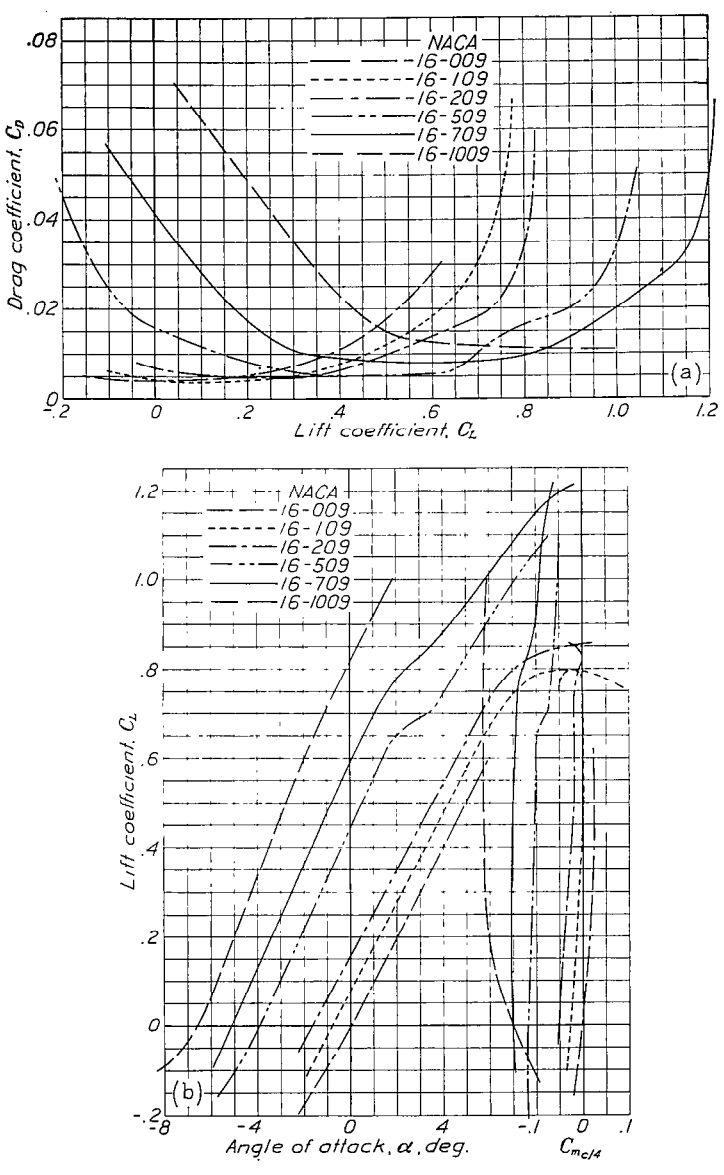

(a) Polar plots.
(b) Lift and moment data.

FIGURE 5.—Aerodynamic characteristics of NACA 16-009-series airfoils. M=0.45.

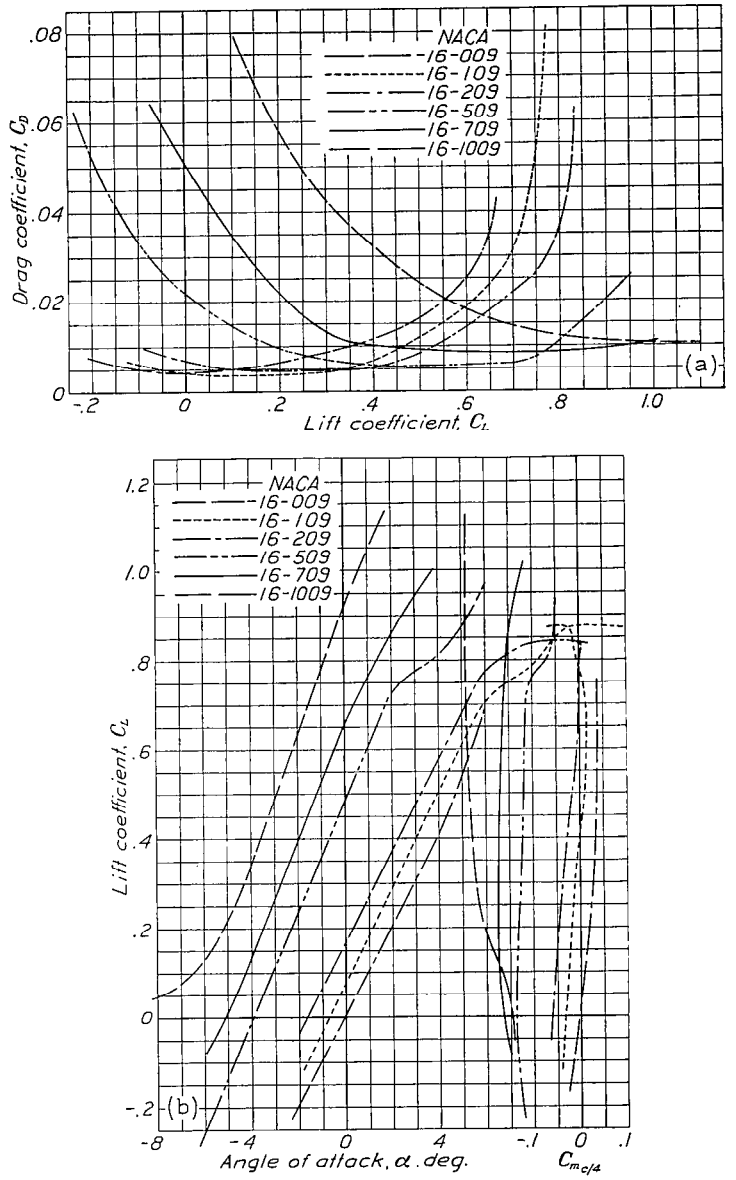

(a) Polar plots.
(b) Lift and moment data.

FIGURE 6.—Aerodynamic characteristics of NACA 16-009-series airfoils. M=0.60.

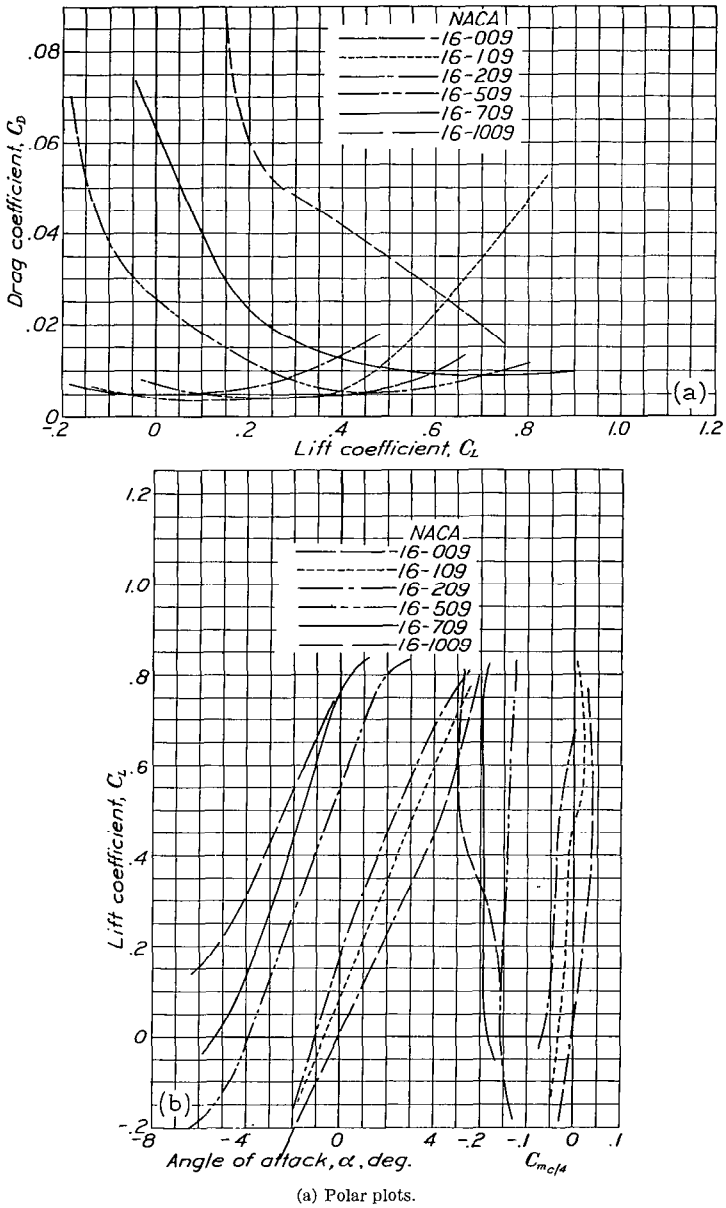

(a) Polar plots.
(b) Lift and moment data.

FIGURE 7.—Aerodynamic characteristics of NACA 16-009-series airfoils. $M=0.70$.

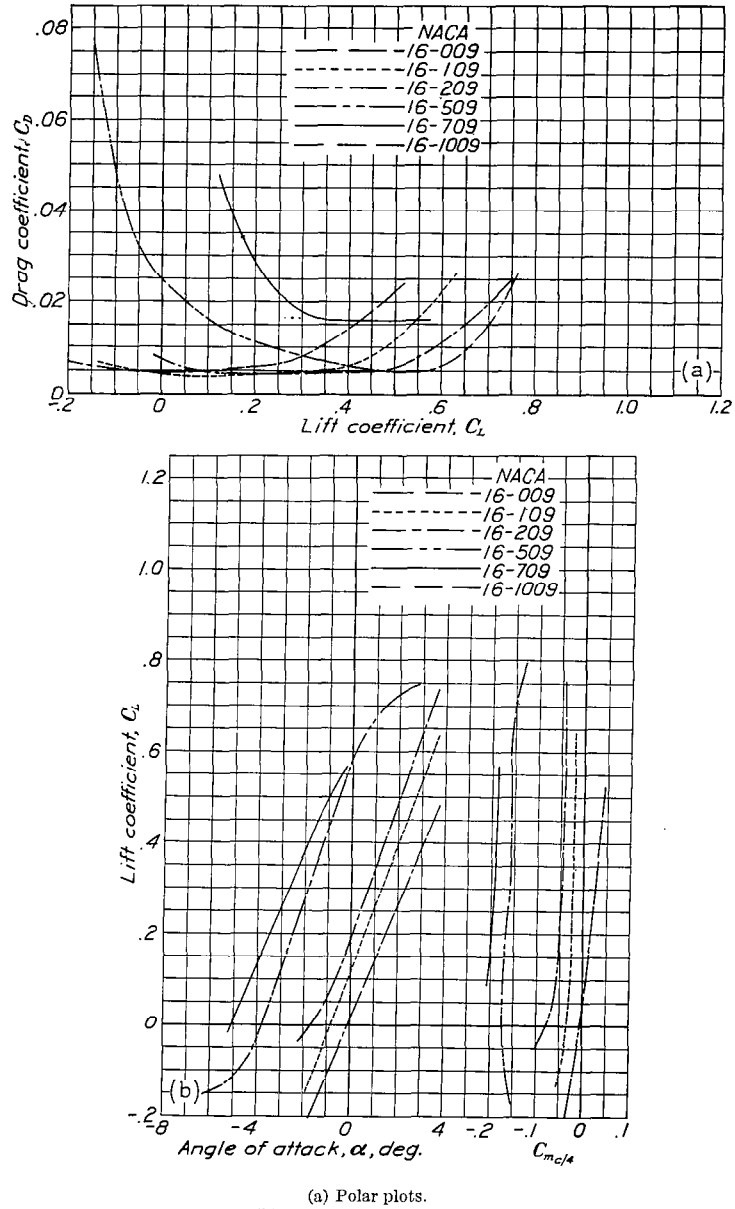

(a) Polar plots.
(b) Lift and moment data.

FIGURE 8.—Aerodynamic characteristics of NACA 16-009-series airfoils. $M=0.75$.

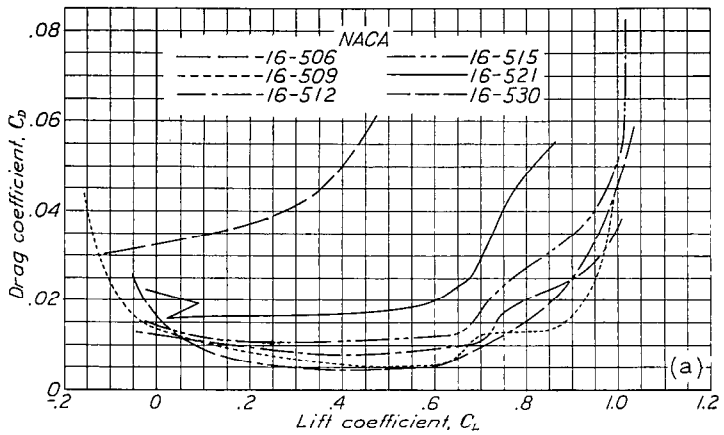

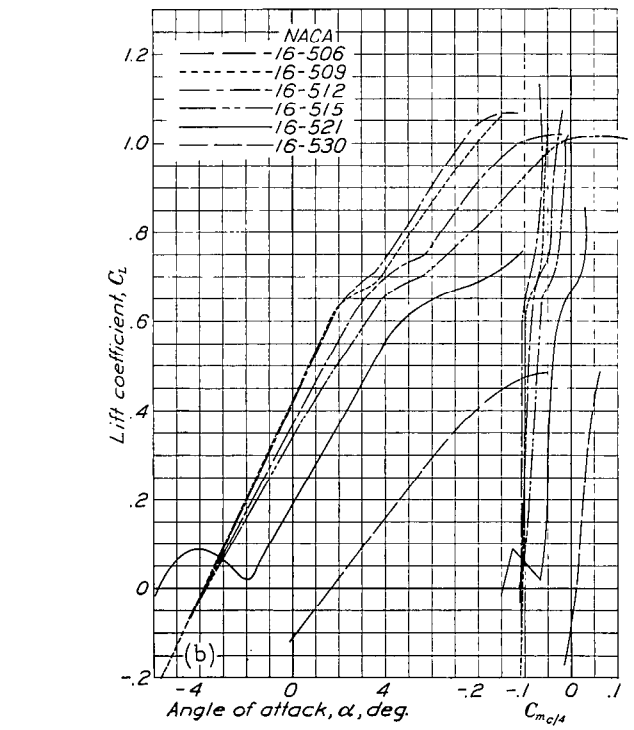

(a) Polar plots.
(b) Lift and moment data.

FIGURE 9.—Aerodynamic characteristics of NACA 16-500-series airfoils. M=0.30.

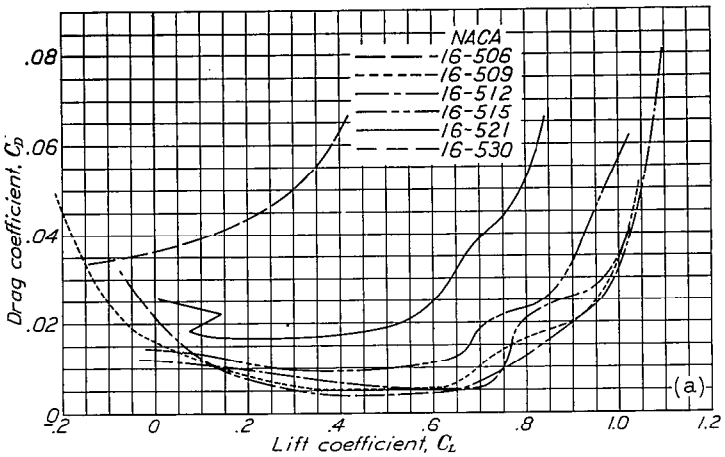

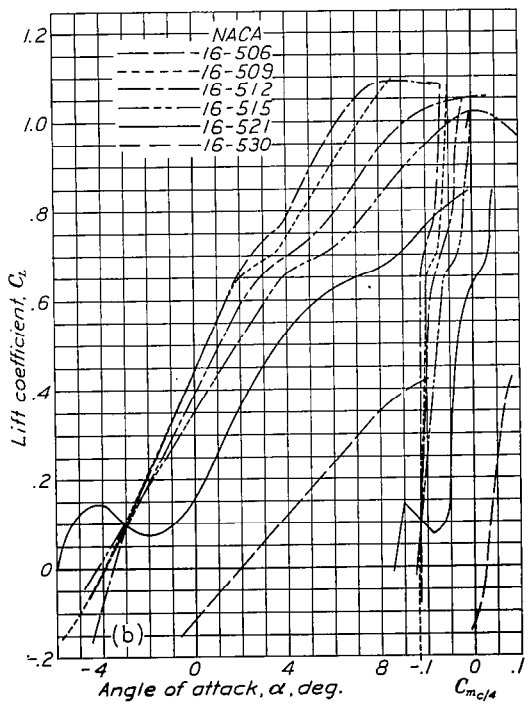

(a) Polar plots.
(b) Lift and moment data.

FIGURE 10.—Aerodynamic characteristics of NACA 16-500-series airfoils. M=0.45.

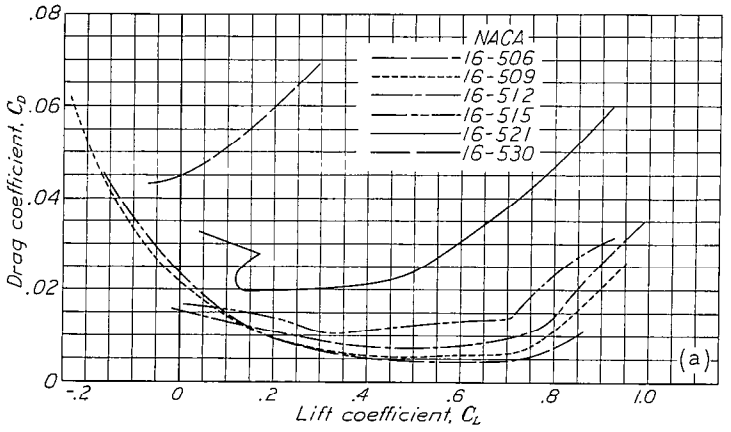

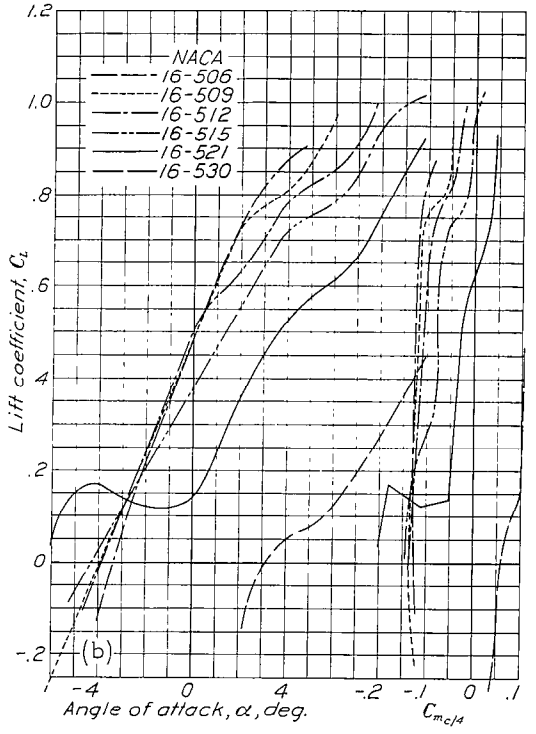

(a) Polar plots.
(b) Lift and moment data.

FIGURE 11.—Aerodynamic characteristics of NACA 16-500-series airfoils. M=0.60.

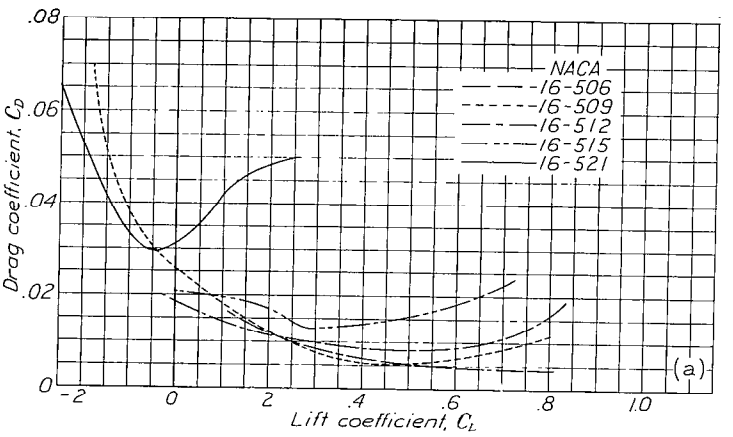

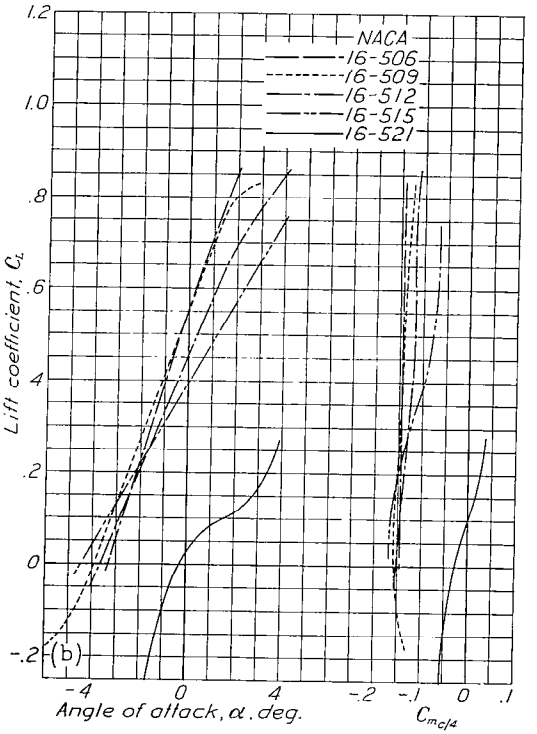

(a) Polar plots.
(b) Lift and moment data.

FIGURE 12.—Aerodynamic characteristics of NACA 16-500-series airfoils. M=0.70.

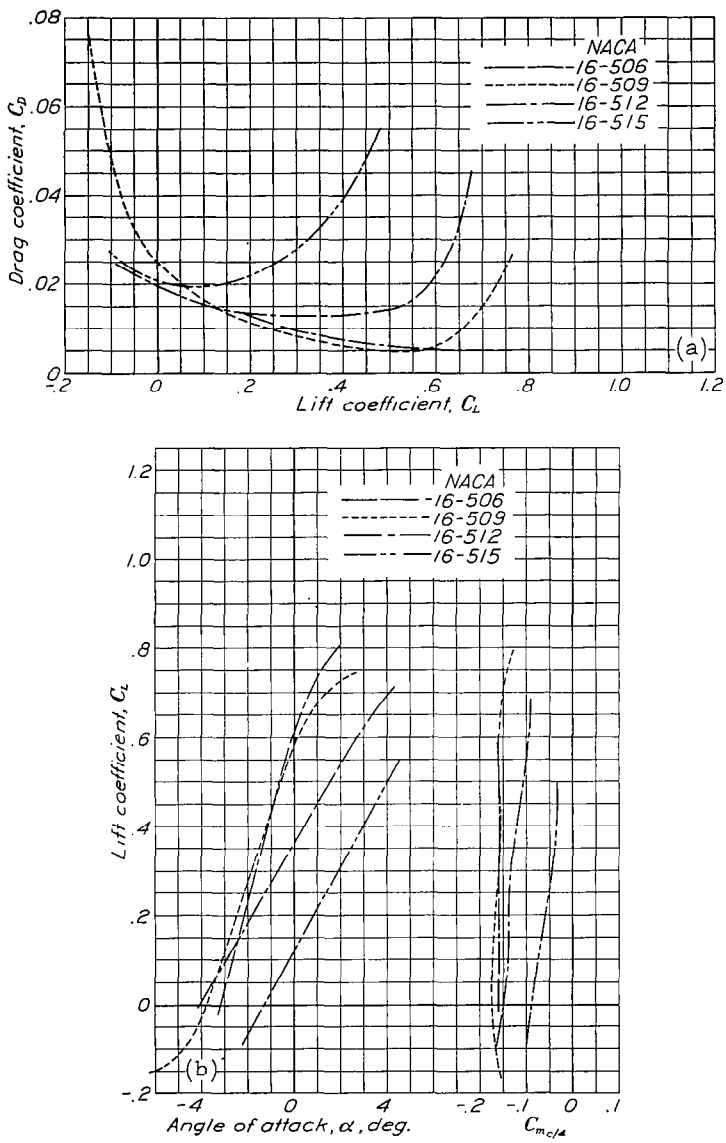

(a) Polar plots.
(b) Lift and moment data.

FIGURE 13.—Aerodynamic characteristics of NACA 16-500-series airfoils. M=0.75.

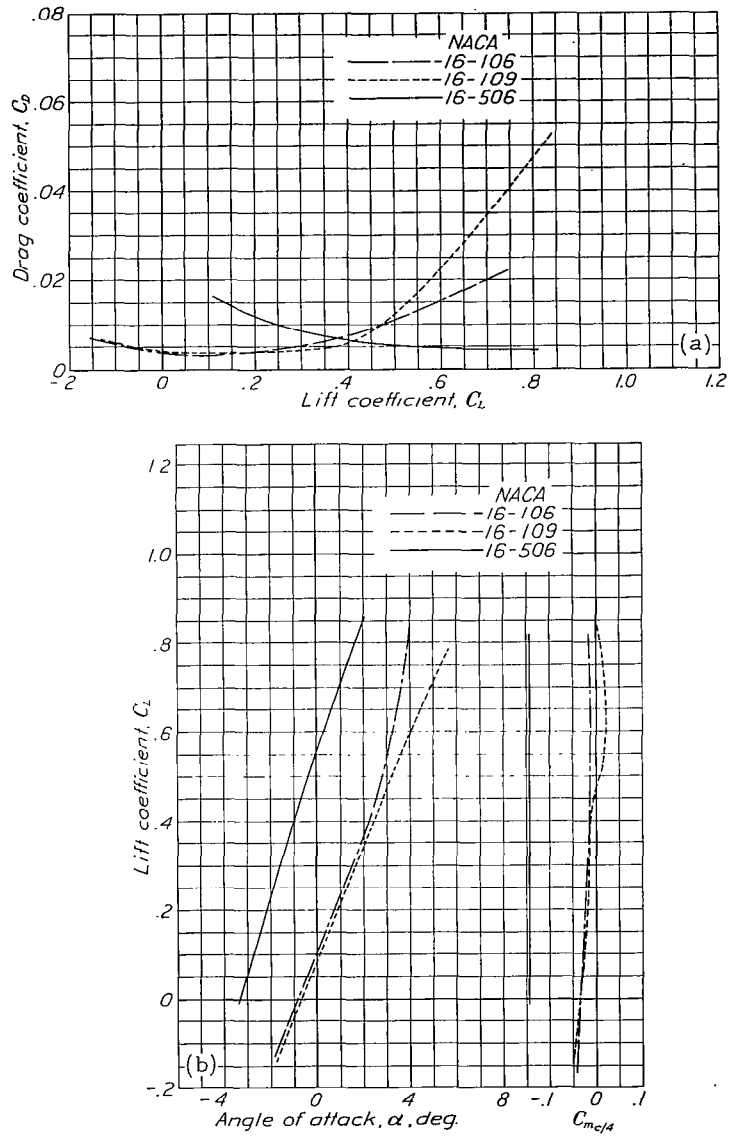

(a) Polar plots.
(b) Lift and moment data.

FIGURE 14.—Aerodynamic characteristics of NACA 16-000-series airfoils. M=0.30.

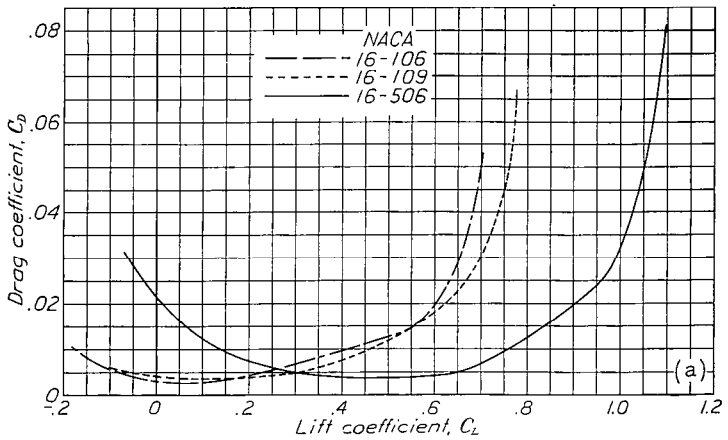

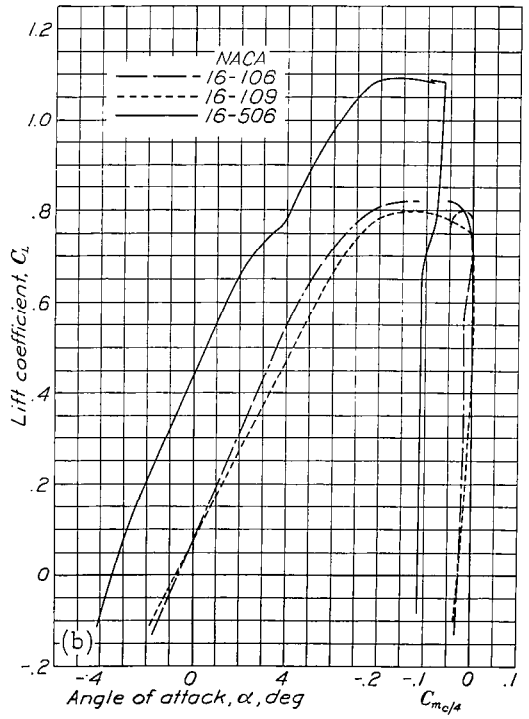

(a) Polar plots.
(b) Lift and moment data.

FIGURE 15.—Aerodynamic characteristics of NACA 16-000-series airfoils. M=0.45.

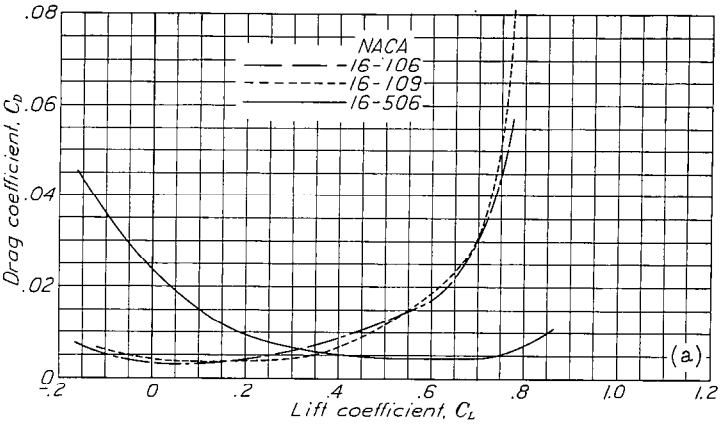

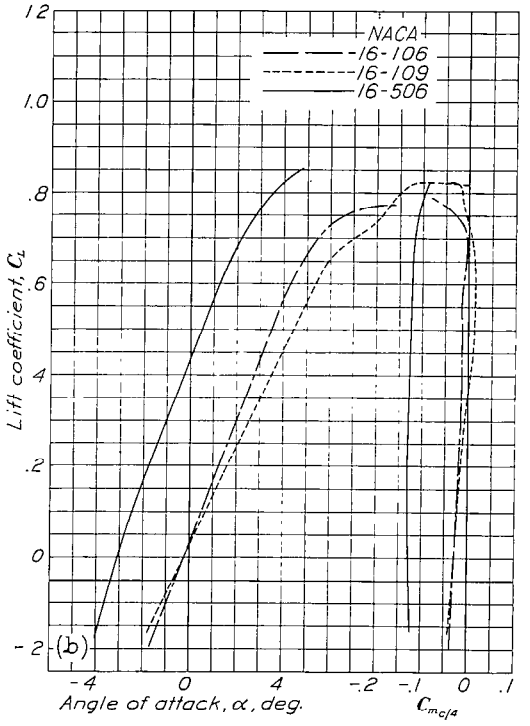

(a) Polar plots.
(b) Lift and moment data.

FIGURE 16.—Aerodynamic characteristics of NACA 16-000-series airfoils. M=0.60.

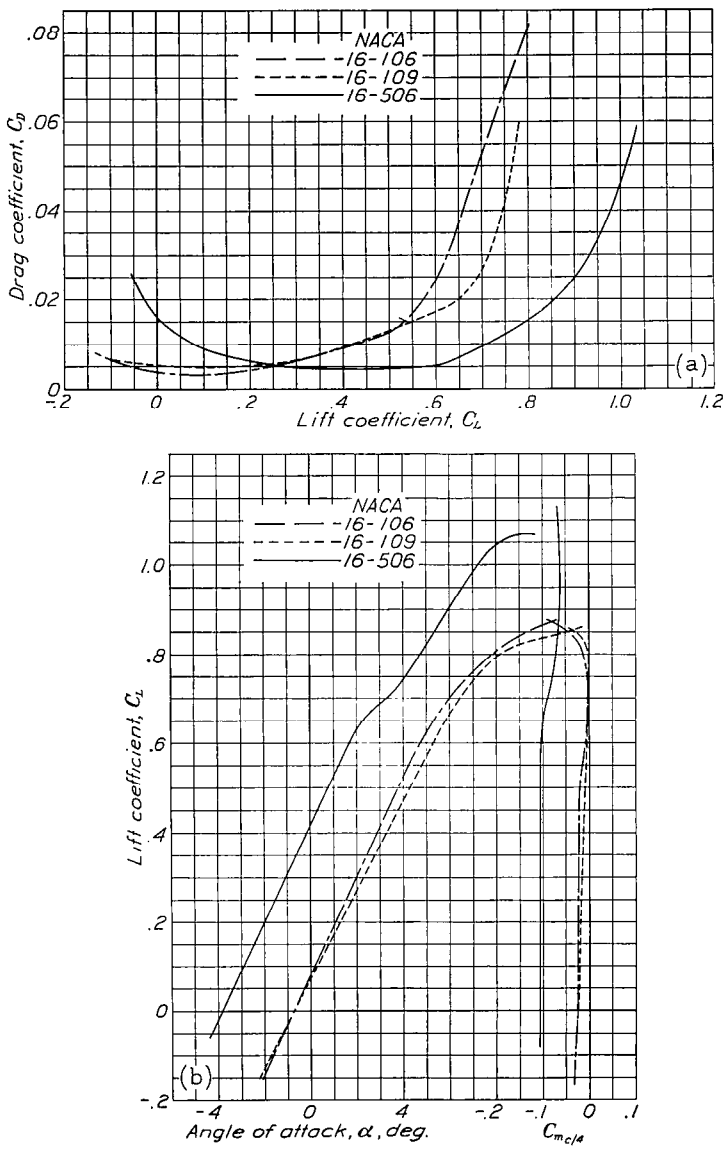

(a) Polar plots.
(b) Lift and moment data.

FIGURE 17.—Aerodynamic characteristics of NACA 16-000-series airfoils. M=0.70.

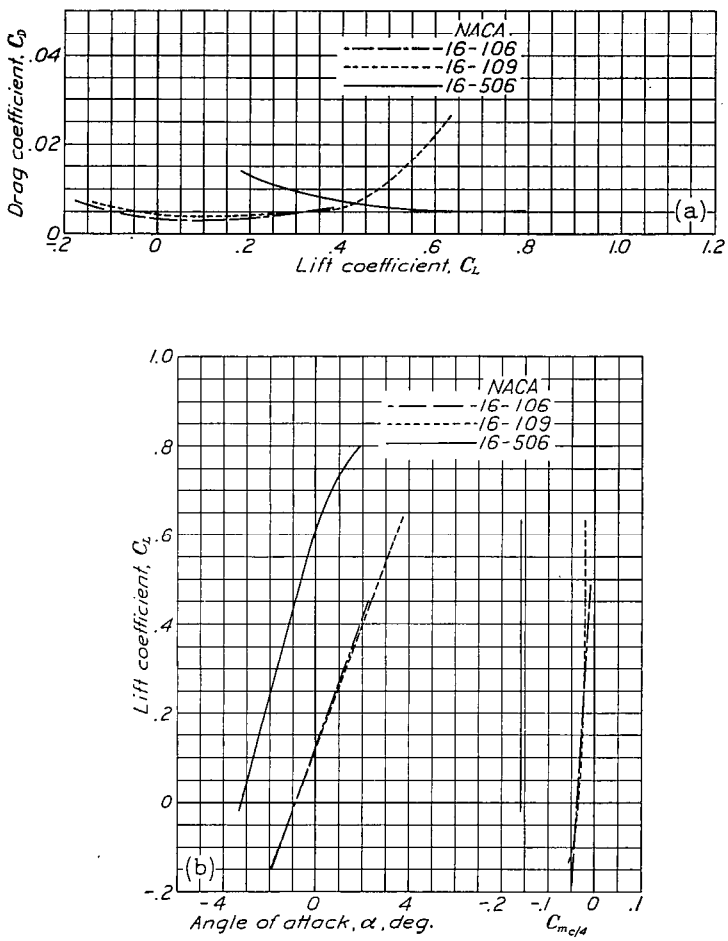

(a) Polar plots.
(b) Lift and moment data.

FIGURE 18.—Aerodynamic characteristics of NACA 16-000-series airfoils. M=0.75.

The departures may be important if variation from the ideal pressure distribution is rapid with change in lift coefficient. This effect, if great, would tend to cause lower drag and higher critical speed for a narrow region near the design condition than are shown by these data. These departures also increase with the airfoil thickness.

The differences between the design conditions and the actual test results may be expected because of the simplifying assumptions of the thin-airfoil theory. Theoretically, it is assumed that the induced velocities are negligibly small as compared with the stream velocity. For thin airfoils at low lifts, this approximation is valid. With increases of lift or thickness, however, the induced velocities approach and sometimes exceed the stream velocity. Study of these effects appears to be very important in order to obtain the proper airfoils for high lift coefficients and large thickness ratios. Deviations shown by the airfoils in this series having high lift and high thickness ratios appear to indicate that the use of a single basic shape is unwarranted if it is desired to obtain optimum airfoils for a wide range of lift coefficient and thickness distribution.

Theoretical pressure-distribution diagrams for the thicker airfoils showed much greater slope of the pressure curve than is shown by the basic NACA 16–009 airfoil. Preliminary study indicated that increasing the leading-edge radius and the fullness of the airfoil between the leading edge and the maximum ordinate may lead to considerable improvement over the thicker airfoils herein reported.

Comparison of airfoils.—Figures 19 and 20 illustrate the differences in aerodynamic characteristics between older propeller-blade sections and the NACA 16-series airfoils. At lower speeds (M=0.45, fig. 19) the 3C8 airfoil appears to attain a much higher maximum lift coefficient than the new airfoils. This result is important in that the wider useful angle-of-attack range may frequently be required to prevent stalling of a propeller during take-off. Over the normal flight range, however, and in most cases for which rational choice of section can be made, the lower drag of the new sections offers considerable opportunity to achieve higher efficiencies. The low drag attained by the NACA 2409–34 airfoil developed from earlier tests in the Langley 11-inch high-speed tunnel may appear surprising. Actually the type of flow for this airfoil approaches the flow that might be expected for the NACA 16–309 airfoil.

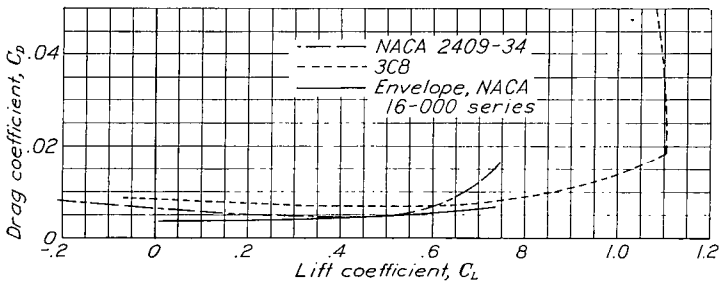

FIGURE 19.—Comparison of airfoils. M=0.45.

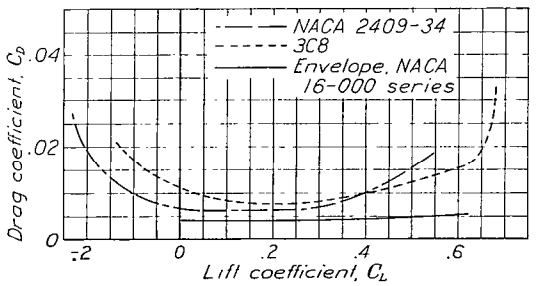

FIGURE 20.—Comparison of airfoils. M=0.75.

The low drag common to most of the NACA 16-series airfoils is associated with more extensive regions of laminar flow in the boundary layer resulting from the rearward position of the point of maximum negative pressure. Unfortunately, however, the Reynolds number is so low that effects of laminar separation may appear and some pressure drag might occur. The small differences in drag between the envelope polar for the new airfoils and for the NACA 2409–34 airfoil are probably a result of this phenomenon. Actually the point of maximum negative pressure for the new airfoils is considerably farther back than the corresponding point for the NACA 2409–34 airfoil but, if laminar separation occurs early, nearly equal drag coefficients might be expected.

At high speeds (M=0.75, fig. 20), the region for which the NACA 16-series airfoils were designed, the superiority of the new airfoils is clear. The earlier onset of the compressibility effects for the older airfoils leads to early drag increases and lower maximum lift coefficients. At speeds above M=0.75 the use of the older sections appears unwarranted for any purpose.

Critical speed.—The variation of the critical speed with lift coefficient and with thickness is given in figures 21 and 22, respectively. These curves indicate that critical speeds exceeding the theoretical values were attained in the tests. In the choice of the test critical speeds, the values were selected on the basis of earlier experience that indicated some rise in drag before large flow disturbances occurred. If these speeds were chosen as the highest values reached before any appreciable drag increment occurred, the agreement with the theoretical curves would be very good. For comparison the critical speed of the 3C8 airfoil is plotted in figure 21. The difference between the new and the older airfoils is greater than shown by the curves because the 3C8 is 8 percent thick, or 1 percent of the chord thinner than the airfoils of the NACA 16–009 series.

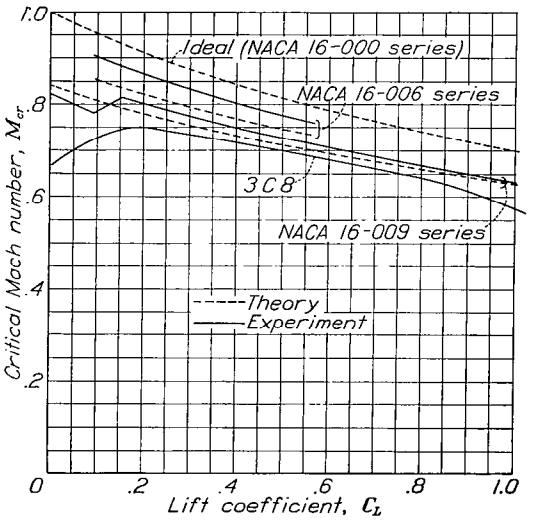

FIGURE 21.—Variation of airfoil critical Mach number with lift coefficient.

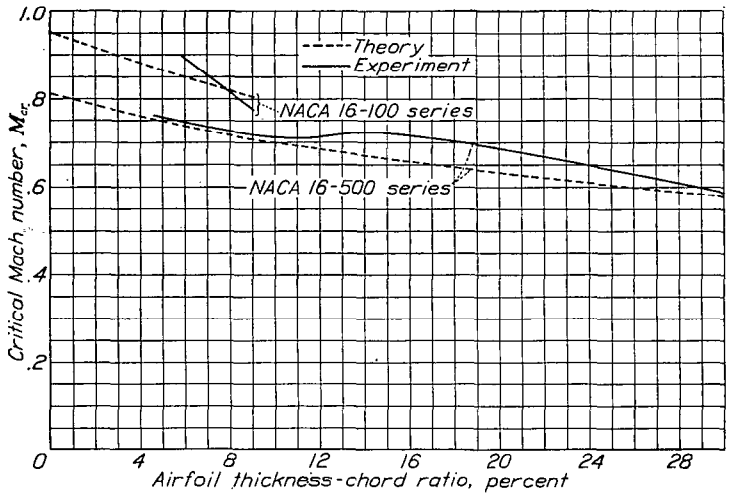

FIGURE 22.—Variation of airfoil critical Mach number with thickness-chord ratio.

Minimum drag.—Coefficients of minimum drag plotted against Reynolds number are given in figures 23 and 24. The lowest drag coefficient was obtained for the NACA 16–106 airfoil; this coefficient is approximately 0.0026 at low speeds and increases to approximately 0.0032 immediately below the critical speed. Of the 9-percent-thick airfoil series designed to operate at various lift coefficients, the NACA 16–109 airfoil appears to have the lowest drag. This result is contrary to expectation because the symmetrical or basic form of the NACA 16–009 would normally have the lowest minimum drag coefficient. The difference may be due to some irregularity of the airfoil surface.

The comparison of the minimum drag coefficients for the 3C8 and the NACA 2409–34 and 16–209 airfoils is shown in figure 25. The high critical speed for the NACA 16–209 airfoil is apparent. The comparison as given directly by figure 25 is a little misleading because of the smaller thickness ratio for the 3C8 airfoil. For equal thickness ratios, the differences between the C-series and the NACA 16-series airfoils will be greater than shown.

Use of the data.—The envelope polars that may be drawn for the NACA 16-series airfoils represent a new and much lower drag as well as higher critical speed attainable for the design of propeller-blade sections. Even though the angle-of-attack range is less than for the older sections, there will be numerous designs for which sufficient angle-of-attack range is given by the new sections. For high-speed, high-altitude aircraft, the advantages of the low drag and high critical speed are of paramount importance and, in these designs, rational choice of section is of increasing importance. In many designs the diameter is fixed by considerations other than propeller efficiency. Thus the induced losses are fixed and propellers of highest efficiency can be developed only by operating and designing the blade sections to operate on the envelope polars. Another important consideration in using new blade sections to achieve highest efficiency concerns the adaptation of the sections to older propeller designs. Optimum efficiency cannot be achieved by simply substituting the new sections for the old on a given design.

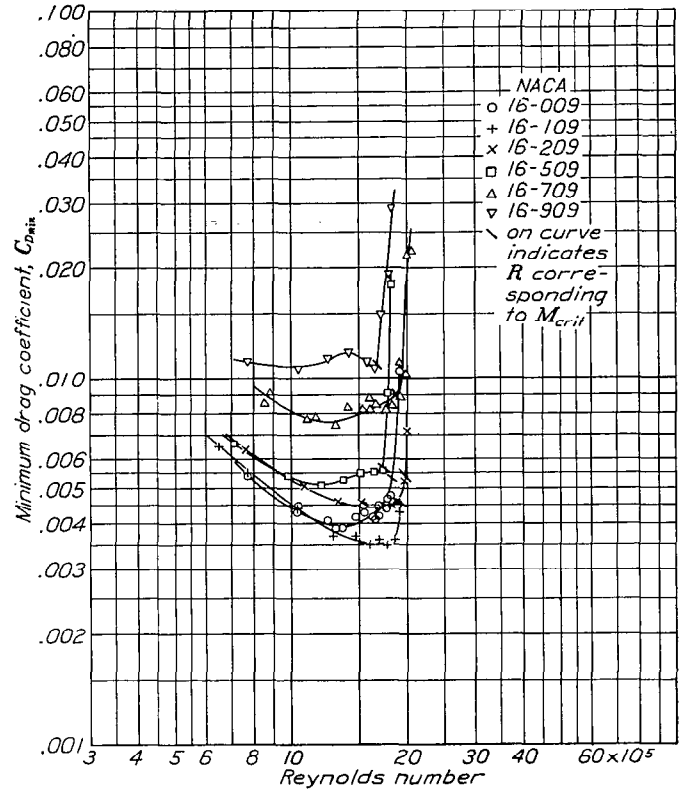

FIGURE 23.—Minimum drag for the NACA 16-009-series airfoils.

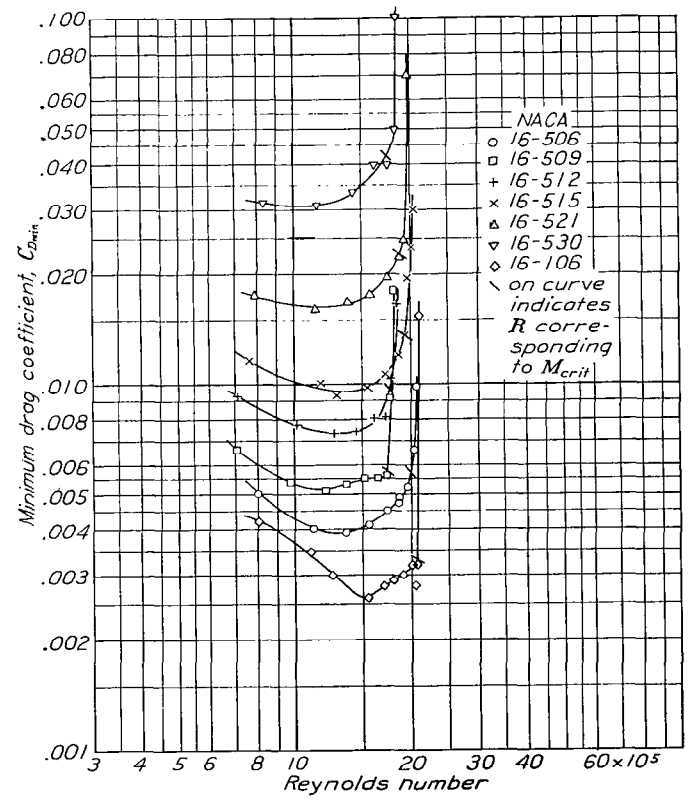

FIGURE 24.—Minimum drag for the NACA 16-500-series airfoils.

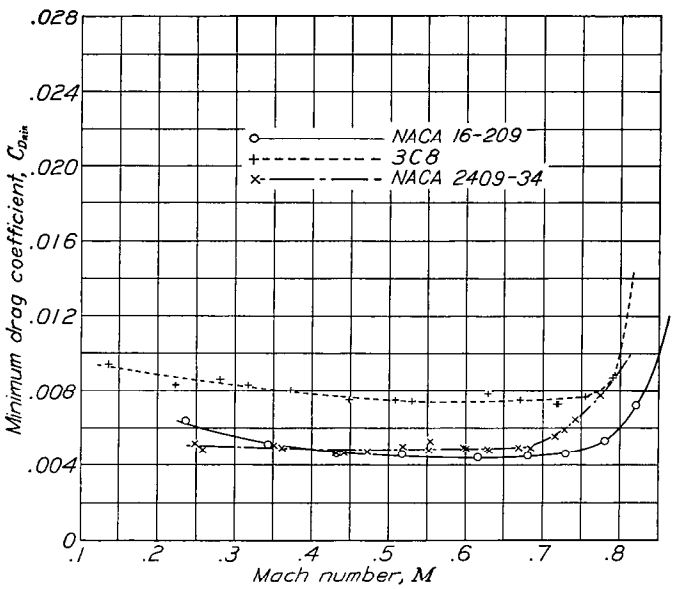

FIGURE 25.—Comparison of airfoil minimum drag coefficients.

The use of better blade sections permits the use of larger diameter and necessitates some plan-form changes. All these factors should be considered in a design for best efficiency with the new blade sections.

CONCLUSION

By a new approach to airfoil design based upon findings of fundamental flow studies, a new series of airfoils, the NACA 16 series, has been developed which has increased critical Mach number and at low speeds reduced drag.

LANGLEY MEMORIAL AERONAUTICAL LABORATORY,
NATIONAL ADVISORY COMMITTEE FOR AERONAUTICS,
LANGLEY FIELD, VA., *June 14, 1939.*

REFERENCES

1. Stack, John: The Compressibility Burble. NACA TN No. 543, 1935.
2. Jacobs, Eastman N.: Methods Employed in America for the Experimental Investigation of Aerodynamic Phenomena at High Speeds. NACA Misc. Paper No. 42, 1936.
3. Stack, John, Lindsey, W. F., and Littell, Robert E.: The Compressibility Burble and the Effect of Compressibility on Pressures and Forces Acting on an Airfoil. NACA Rep. No. 646, 1938.
4. Glauert, H.: The Elements of Aerofoil and Airscrew Theory. Cambridge Univ. Press, 1926, pp. 87–93.
5. Theodorsen, Theodore: Theory of Wing Sections of Arbitrary Shape. NACA Rep. No. 411, 1931.
6. Stack, John, and von Doenhoff, Albert E.: Tests of 16 Related Airfoils at High Speeds. NACA Rep. No. 492, 1934.
7. Stack, John: The N. A. C. A. High-Speed Wind Tunnel and Tests of Six Propeller Sections. NACA Rep. No. 463, 1933.
8. Jacobs, Eastman N., Ward, Kenneth E., and Pinkerton, Robert M.: The Characteristics of 78 Related Airfoil Sections from Tests in the Variable-Density Wind Tunnel. NACA Rep. No. 460, 1933.

U. S. GOVERNMENT PRINTING OFFICE: 1947

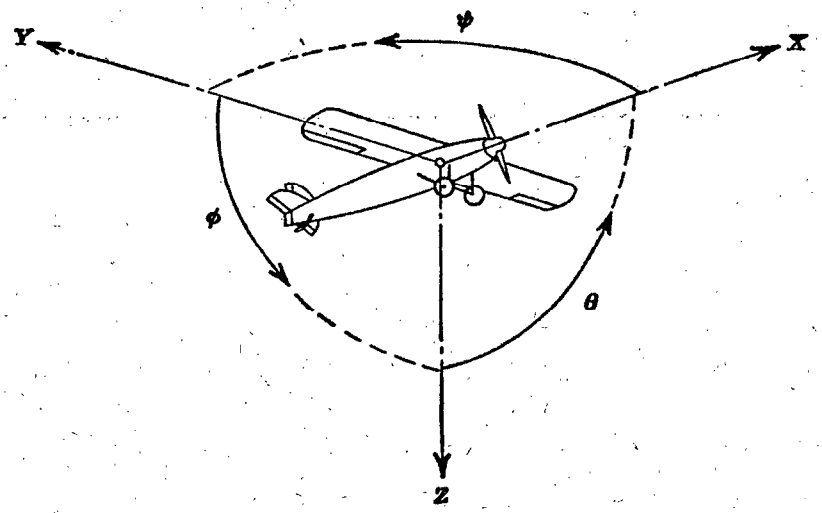

Positive directions of axes and angles (forces and moments) are shown by arrows

Axis		Force (parallel to axis) symbol	Moment about axis			Angle		Velocities	
Designation	Symbol		Designation	Symbol	Positive direction	Designation	Symbol	Linear (component along axis)	Angular
Longitudinal	X	X	Rolling	L	$Y \longrightarrow Z$	Roll	φ	u	p
Lateral	Y	Y	Pitching	M	$Z \longrightarrow X$	Pitch	θ	v	q
Normal	Z	Z	Yawing	N	$X \longrightarrow Y$	Yaw	ψ	w	r

Absolute coefficients of moment

$C_l = \frac{L}{qbS}$ (rolling) $\quad C_m = \frac{M}{qcS}$ (pitching) $\quad C_n = \frac{N}{qbS}$ (yawing)

Angle of set of control surface (relative to neutral position), δ. (Indicate surface by proper subscript.)

4. PROPELLER SYMBOLS

D Diameter

p Geometric pitch

p/D Pitch ratio

V' Inflow velocity

V_s Slipstream velocity

T Thrust, absolute coefficient $C_T = \frac{T}{\rho n^2 D^4}$

Q Torque, absolute coefficient $C_Q = \frac{Q}{\rho n^2 D^5}$

P Power, absolute coefficient $C_P = \frac{P}{\rho n^3 D^5}$

C_s Speed-power coefficient $= \sqrt[5]{\frac{\rho V^5}{P n^2}}$

η Efficiency

n Revolutions per second, rps

Φ Effective helix angle $= \tan^{-1}\left(\frac{V}{2\pi r n}\right)$

5. NUMERICAL RELATIONS

1 hp=76.04 kg-m/s=550 ft-lb/sec

1 metric horsepower=0.9863 hp

1 mph=0.4470 mps

1 mps=2.2369 mph

1 lb=0.4536 kg

1 kg=2.2046 lb

1 mi=1,609.35 m=5,280 ft

1 m=3.2808 ft